A R C H I V E S O F M E T A L L U R G Y A N D M A T E R I A L S
Volume 60 2015 Issue 4
DOI: 10.1515/amm-2015-0436

M. WRÓBEL*, A. BURBELKO*#, D. GURGUL*

MODELLING OF CHANGE IN DENSITY OF NODULAR CAST IRON DURING SOLIDIFICATION USING CELLULAR AUTOMATON

MODELOWANIE ZMIAN GĘSTOŚCI ŻELIWA SFEROIDALNEGO PODCZAS KRYSTALIZACJI ZA POMOCĄ AUTOMATU KOMÓRKOWEGO

Density change occurring in ductile iron castings is a phenomenon far more complicated than in other casting alloys. Initially, graphite nodules grow directly from liquid phase. That is the reason for decrease in alloy density and casting expansion. Decaying carbon concentration in liquid phase adjacent to graphite nodules favours growth of austenite, which covers them isolating from the liquid. In order for graphite to grow further diffusion of carbon through thickening solid solution layer is needed. At this time expansion fades and shrinkage begins. Industrial experience shows that whether or not shrinkage defects in ductile iron castings will occur depends on wall thickness.

In the paper an attempt to identify mechanism of shrinkage porosity formation in nodular iron castings during solidification was made. To that end a two-dimension simulation of binary Fe-C system solidification by cellular automaton method was carried out. Using data obtained with Thermo-CALC software, dependencies of temperature on density for each present phase were determined. For liquid phase and austenite influence of carbon concentration on density was also appended. Applying those relationships to the model, density of each individual cell of used grid as well as mean value for whole analysed region were assessed. The method allowed to consider volume fractions of phases and heterogeneity of solid and liquid solutions to find the mean density of the material.

The paper presents results of computer simulation of nodular iron density change, with eutectic saturation of 0,9 to 1,1.

Keywords: Nodular Iron, Shrinkage, Expansion, CALPHAD, Solidification modelling.

Zmiany objętościowe zachodzące w odlewach z żeliwa sferoidalnego są zjawiskiem znacznie bardziej złożonym, niżeli w innych stopach odlewniczych. Początkowo krystalizacja kulek grafitu, która jest przyczyną zmniejszenia gęstości i występowania rozszerzalności przedskurczowej, przebiega bezpośrednio z fazy ciekłej. Zmniejszenie zawartości węgla w cieczy przylegającej do kulek grafitu sprzyja krystalizacji austenitu, którego warstwa izoluje te cząstki od cieczy. Dalszy wzrost grafitu wymaga dyfuzji węgla przez rosnącą warstwę roztworu stałego. Na tym etapie krystalizacji rozszerzalność zanika i zaczyna się skurcz. Z praktyki przemysłowej wiadomo, że o występowaniu wad skurczowych w odlewach z żeliwa sferoidalnego o takim samym składzie chemicznym decyduje grubości ścianki.

W pracy podjęto próbę zidentyfikowania mechanizmu tworzenia się wad skurczowych w odlewach z żeliwa sferoidalnego podczas krystalizacji. W tym celu przeprowadzono dwuwymiarową symulację krystalizacji podwójnego stopu Fe-C za pomocą modelu wykorzystującego technikę automatu komórkowego. Na podstawie danych otrzymanych przy użyciu oprogramowania Thermo-CALC wyznaczono zależności gęstości poszczególnych faz występujących w układzie od temperatury, a dla roztworu ciekłego i stałego dodatkowo od stężenia węgla. Za pomocą otrzymanych zależności wyznaczano gęstość w poszczególnych komórkach stosowanej siatki obliczeniowej oraz średnią gęstość analizowanego obszaru. Metoda ta pozwoliła wyznaczyć gęstość materiału z uwzględnieniem udziałów objętościowych poszczególnych faz i niejednorodności roztworów ciekłego i stałego.

W pracy przedstawiono wyniki symulacji komputerowej zmian objętościowych żeliwa sferoidalnego o stopniu nasycenia eutektycznego w granicach od 0,9 do 1,1.

1. Introduction

It is known that expansion of the ductile iron (DI) is few times greater than that with flake graphite [1]. As a result of increase in volume, due to precipitation of graphite in the initial stage of solidification, metallostatic pressure may rise [2]. If the mould isn't rigid enough it leads to irreversible deformation of its walls (swelling of the mould) [3]. Such distortion is considered to be one of the reasons for shrinkage defects, in DI castings solidifying in "vulnerable" moulds, to occur.

Growth conditions of graphite in DI compared to other cast iron grades differs considerably. In grey iron both primary and

* UNIVERSITY OF SCIENCE AND TECHNOLOGY AGH, FACULTY OF FOUNDRY ENGINEERING, AL. A. MICKIEWICZA 30, 30-059 KRAKÓW, POLAND
# Corresponding author: abur@agh.edu.pl

eutectic graphite have continuous access to diminishing liquid phase. Additionally eutectic graphite, during solidification, growths with constant contact of three phases.

In DI globules of primary and eutectic graphite, in the initial stage of solidification, don't have contact with austenite grains and grow directly form liquid phase [4, 5]. Later on grains of those two phases connect. The layer of austenite momentarily isolates graphite from the liquid. In order for graphite to grow further, diffusion of carbon from liquid through austenite shell must occur.

Probably that is the reason for shrinkage phenomena in DI castings to be more complicated than in other alloys.

Experience of making DI castings in Odlewnie Polskie S. A. confirms known from literature signs of shrinkage defects in castings made of this alloy [3]:

1. mechanism of feeder's effect is far more complicated than in alloys that do not show expansion phenomenon; sometimes by eliminating the feeders one can observe a decrease in porosity;
2. minimal porosity occurs in eutectic alloys, wherein it is beneficial to increase eutectic's carbon content – while preserving eutectic saturation (S_c) equal to 1,0;
3. porosity of grey iron castings is much smaller than of those made of DI.

Mechanisms of shrinkage defects formation continue to be the subject of discussions, but it is obvious that the main reason for that is change in volume of an alloy during cooling and phase transformations. To know those mechanisms, solidification modelling – with consideration of change in density – may show to be very useful tool. In order to get exact values of volume changes the relations of each of DI phase's density with respect to temperature and for liquid phase and austenite also with respect to carbon concentration were determined.

Computations, basing on CALPHAD method – a technique of thermodynamic calculations – were performed suing Thermo-Calc Software. Basics on the CALPHAD method can be found in [6, 7]. For solidification simulation the Cellular Automata method was used [5, 8, 9, 10].

2. Density calculations

2.1. Considered ranges of carbon concentration and temperature

Computer simulation of volume changes of DI with eutectic saturation (S_c) ranging from 0,9 to 1,1 were performed. In order to delimit carbon concentration and temperature for defining liquid phase's density the following steps were undertaken. For extreme values of S_c the carbon concentration was determined and the range, rounded to the one tenth, of 3,9 ÷ 4,8 wt. % was accepted. The highest liquidus temperature in this concentration limits happens for extremely hypereutectic alloy and is equal to ca. 1332°C. Wide range of temperature was chosen: from 1000°C (that is considerably lower than temperature of eutectic transformation) up to 1400°C.

Making use of Fe-C binary phase diagram, the range of temperature (950 ÷ 1350°C) and carbon concentration (1,0 ÷ 2,1 wt. %) for austenite was selected. Within those ranges lies the field of solid solution corresponding to carbon concentration of entire alloy. Density of graphite was calculated in the same temperature range.

Fig. 1 illustrates dependence of graphite's density on temperature, Fig. 2 and Fig. 3 shows calculation results of density for liquid phase and austenite in appropriate limits of carbon concentration and temperature.

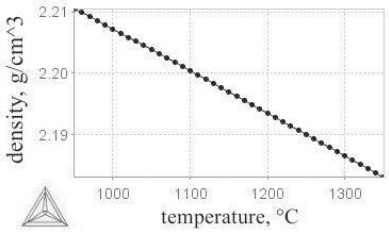

Fig. 1. Dependency of graphite's density on temperature

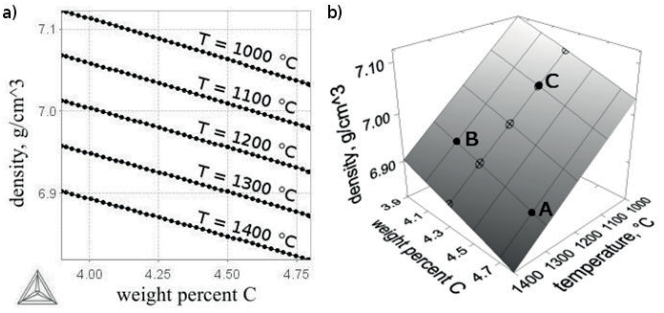

Fig. 2. Dependency of liquid phase's density on temperature and carbon concentration on 2D (a) and 3D (b) plot. Coordinates of points A, B, C were used to determine equation of the plane

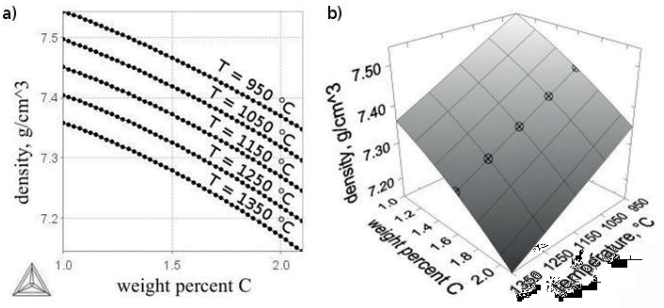

Fig. 3. Dependency of austenite's density on temperature and carbon concentration on 2D (a) and 3D (b) plot

2.2. Functions of density of each phase

Linear dependence of graphite's density on temperature (Fig. 1) is described by Eq. (1):

$$\rho_{gra} = -6{,}9 \cdot 10^{-5} \cdot T + 2{,}276 \qquad (1)$$

where temperature is in °C and density has units of g/cm^3.

For liquid phase and austenite the density is a function of 2 variables. The influence of carbon concentration on liquid's density is linear, for austenite more exact is quadratic function. Equal intervals between next isotherms in sections (a) in Fig. 2 and Fig. 3 suggest linear dependency of density on

temperature, keeping constant carbon concentration, for this phases. In order to verify the above, calculations of density for carbon concentration of 4,3 in liquid and 1,6 wt. % in austenite (marked points in sections (b)) were performed, the results, confirming linear dependencies, are shown in Fig. 4 and Fig. 5.

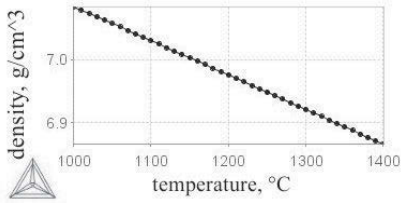

Fig. 4. Dependency of liquid phase's density on temperature for fixed carbon concentration: 4,3 wt. %

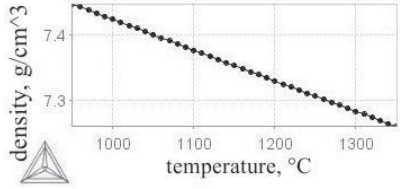

Fig. 5. Dependency of austenite's density on temperature for fixed carbon concentration: 1,6 wt. %

Proportionality of density to temperature and carbon concentration in liquid phase allows to describe this dependency by the equation of the plane. The points chosen to determine this dependence are marked in Fig. 2 (b) – coordinates are given in TABLE 1.

TABLE 1
Coordinates of the points used to determine equation of the plane corresponding to density of the liquid phase

point	wt. % C	Temperature, °C	density, g/cm^3
A	4.7	1300	6,882
B	4.1	1300	6,939
C	4.3	1100	7,030

Found plane equation has the form of Eq. (2):

$$\rho_{liq} = -9{,}5 \cdot 10^{-2} \cdot w(C) - 5{,}5 \cdot 10^{-4} \cdot T + 8{,}042 \qquad (2)$$

where $w(C)$ is the carbon concentration stated in wt. %.

Due to nonlinear dependency of austenite's density on carbon concentration, describing the surface in Fig. 3 (b) using equation of the plane would lead to considerable calculation error. To avoid the inaccuracy, the other description was proposed, possible to employ thanks to proportionality of solid solution's density to the temperature. Dependency of austenite's density on carbon concentration – for isotherm 1150°C (Fig. 3 (a))– was described by the second-degree polynomial, Eq. (3):

$$\left[\rho_{fcc}\right]_{T=1150°C} = -5 \cdot 10^{-2} \cdot \left[w(C)\right]^2 - 3{,}17 \cdot 10^{-2} \cdot w(C) + 7{,}532 \qquad (3)$$

Next the equation of line parallel to one on Fig. 5 with a zero at 1150°C was determined:

$$\Delta\rho_{fcc} = -4{,}7 \cdot 10^{-4} \cdot T + 0{,}54 \qquad (4)$$

where:

$$\Delta\rho_{fcc} = [\rho_{fcc}]_{w(C)=1,6} - [\rho_{fcc}]_{w(C)=1,6;T=1150°C} \qquad (5)$$

Combining Eq. (3) and Eq. (4) the following form of austenite's dependency on carbon concentration and temperature was obtained, Eq. (6):

$$\rho_{fcc} = -5 \cdot 10^{-2} \cdot \left[w(C)\right]^2 - 3{,}17 \cdot 10^{-2} \cdot w(C) - 4{,}7 \cdot 10^{-4} \cdot T + 8{,}072 \qquad (6)$$

2.3. Verification of designated formulae

Using Thermo-Calc Software, density of each phase, with accuracy of 0,001 g/cm3 at the nodes of the grid, with parameters shown in TABLE 2, was calculated. The differences ($\Delta\rho$) between thermodynamic calculations and values of density obtained using proposed Eqs. (1), (2) and (6) were computed. The maximal differences were put in TABLE 2 as well.

TABLE 2
Parameters of inspected zones together with maximal errors for each phase

		graphite	liquid phase	austenite
Temperature range, °C	min	950	1000	950
	max	1350	1400	1350
Temperature step, °C		10	100	100
Carbon concentration range, wt. %	min	–	3,9	1,0
	max	–	4,8	2,1
Carbon concentration step, wt. %		–	0,05	0,025
Maximal error $\Delta\rho$, g/cm^3		< 0,001	0,004	0,010

As suspected, the biggest error occurs for the most complicated dependency – austenite. It is noteworthy that the maximum (max $\Delta\rho$) happens in the regions with carbon concentration above highest solubility at certain temperature (Fig. 6), and within single-phase austenite field inaccuracy does not exceed 0,003 g/cm^3.

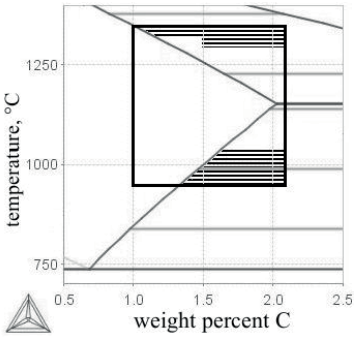

Fig. 6. Fragment of Fe-C phase diagram, field inside marked rectangle indicates considered in calculations range of temperature and carbon concentration. Lined field marks zone with biggest error $\Delta\rho$

3. Results of the modelling

The forecast of density change of DI using solidification model exercising Cellular Automata method was performed. In figure 7 the example of simulation result was presented. Wider description of the model and results obtained using it one can find in [11].

Fig. 7. Microstructure of ductile iron obtained using Cellular Automata model [11]

Carbon concentration in cast iron has significant impact on shrinkage phenomena because amount of graphite in alloy's microstructure depends on its content. It is known that the dependency is extreme. The foundry engineering experience show that minimal level of shrinkage defects occurs in cast iron with eutectic composition. It is considered that in hypoeutectic cast iron, amount of graphite is too small for its expansion to compensate shrinkage of whole alloy. On the other hand in hypereutectic cast iron solidification of the primary graphite grains leads to excessive expansion still before solidification of the eutectic.

In this paper, using computer modelling, the forecast of change in density of binary Fe-C alloy was carried out. Into the model, descriptions of each phase's density by the means of Eqs. (1), (2) and (6), were implemented. Calculations were performed upon two-dimensional grid of 640×640 cells. Cell's edge was 1 μm long. Uniform, initial carbon concentration field in liquid was assumed.

First series of computations was performed for cooling the specimen with constant cooling rate of 10 K/s. Solidification for five values of eutectic saturation (0,90; 0,95; 1,00; 1,05 and 1,10) was modelled. Fig. 8 illustrates influence of change in Sc on solidification time and specific volume of the alloy.

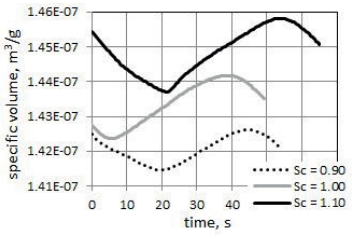

Fig. 8. Influence of eutectic saturation on solidification time and specific volume of modelled alloy

Another series of calculations was carried out for varying cooling rate (T` = 5, 10, and 20 K/s) for fixed Sc = 1,00. Results are shown in Fig. 9.

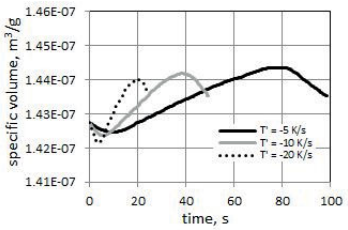

Fig. 9. Influence of cooling rate on solidification time and specific volume of modelled alloy

The forecast of change in density of an alloy was based on information regarding variations of volume fraction of each phase. Density of the cast iron was calculated as weighted average of density of each phase considering whole field of Cellular Automata grid.

As follows from Figs. 8 and 9, in each analysed case, at the beginning of solidification process the shrinkage related to decrease of temperature and crystallization of primary austenite grains occurs. Precipitation of graphite in the second stage, during solidification of the eutectic, effects in expansion, whereas at the final stage of solidification when graphite grows by the means of carbon diffusion through solid phase an expansion shifts to shrinkage.

4. Conclusions

Making use of the CALPHAD method the data were acquired to be used to designate dependencies of graphite, liquid phase and austenite in the binary Fe-C system on the temperature and additionally on carbon concentration for liquid and solid solution. Obtained dependencies were implemented into mathematical model of solidification of DI.

Utilising a tool allowing for solidification modelling application and software for thermodynamic calculations to communicate, would let "on the flight" transfer of the necessary data making the need to obtain functions of density unnecessary. Applying such tool is one of the aims of authors in the study regarding solidification modelling.

Each of presented simulation results show shrinkage of the cast iron, in the initial stage of solidification, related to decrease of temperature, increase of liquid phase's density and crystallization of primary austenite grains. Precipitation of graphite in next stage, during eutectic solidification, leads to expansion, at the final stage, when graphite grains grow by the means of carbon diffusion through austenite an expansion shifts back to shrinkage.

Acknowledgement

This work was supported by AGH statutory project no. 15.11.170.483.

[1] G. Nandori, Materials Science Forum **215-216**, 399 (1996).
[2] Z. Gedeonova *et al.*, Materials Science Forum **215-216**, 391 (1996).
[3] I. Ohnaka *et al.*, International Journal of Cast Metals Research **21**, 11 (2008).
[4] H. Fredriksson, J. Stjerndahl, J. Tinoco, Materials Science and Engineering A **413–414**, 363 (2005).

[5] A. Burbelko *et al.*, Key Engineering Materials **457**, 330 (2011).
[6] P. J. Spencer, CALPHAD **32** 1 (2008).
[7] L. A. Zabdyr, Strategia CALPHAD, Instytut Metalurgii i Inżynierii Materiałowej PAN, Kraków 2005.
[8] A. Burbelko, D. Gurgul, Computer Methods in Materials Science **11**, 128 (2011).
[9] A. Burbelko *et al.*, Archives of Foundry Engineering, **11**, 4, 13 (2011).
[10] D. Gurgul, A. Burbelko, Archives of Metallurgy and Materials **55**,2, 53-56 (2010).
[11] D. Gurgul *et al*., CSSCR2013, Stockholm, Sweden and Helsinki, Finland, May 20-23, 2013.

Received: 20 January 2015.